ADVANCED OPTICAL MATERIALS

Supporting Information

for *Adv. Optical Mater.*, DOI 10.1002/adom.202400259

Highly Efficient Photoanodic Material: Utilizing Dihydrolipoic Acid-Functionalized $CuInS_2$ Quantum Dots in Photoelectrochemical Cells

*Giacomo Morselli, Caterina Bellatreccia, Michele Mazzanti, Vito Cristino, Anna Ianniello, Stefano Caramori, Raffaello Mazzaro and Paola Ceroni**

Supporting Information

Highly Efficient Photoanodic Material: Utilizing Dihydrolipoic Acid-Functionalized $CuInS_2$ Quantum Dots in Photoelectrochemical Cells

*Giacomo Morselli, Caterina Bellatreccia, Michele Mazzanti, Vito Cristino, Anna Ianniello, Stefano Caramori, Raffaello Mazzaro and Paola Ceroni**

Table of Contents

^{1}H and ^{13}C-NMR spectra ($CDCl_3$, 400 MHz) of dihydrolipoic acid

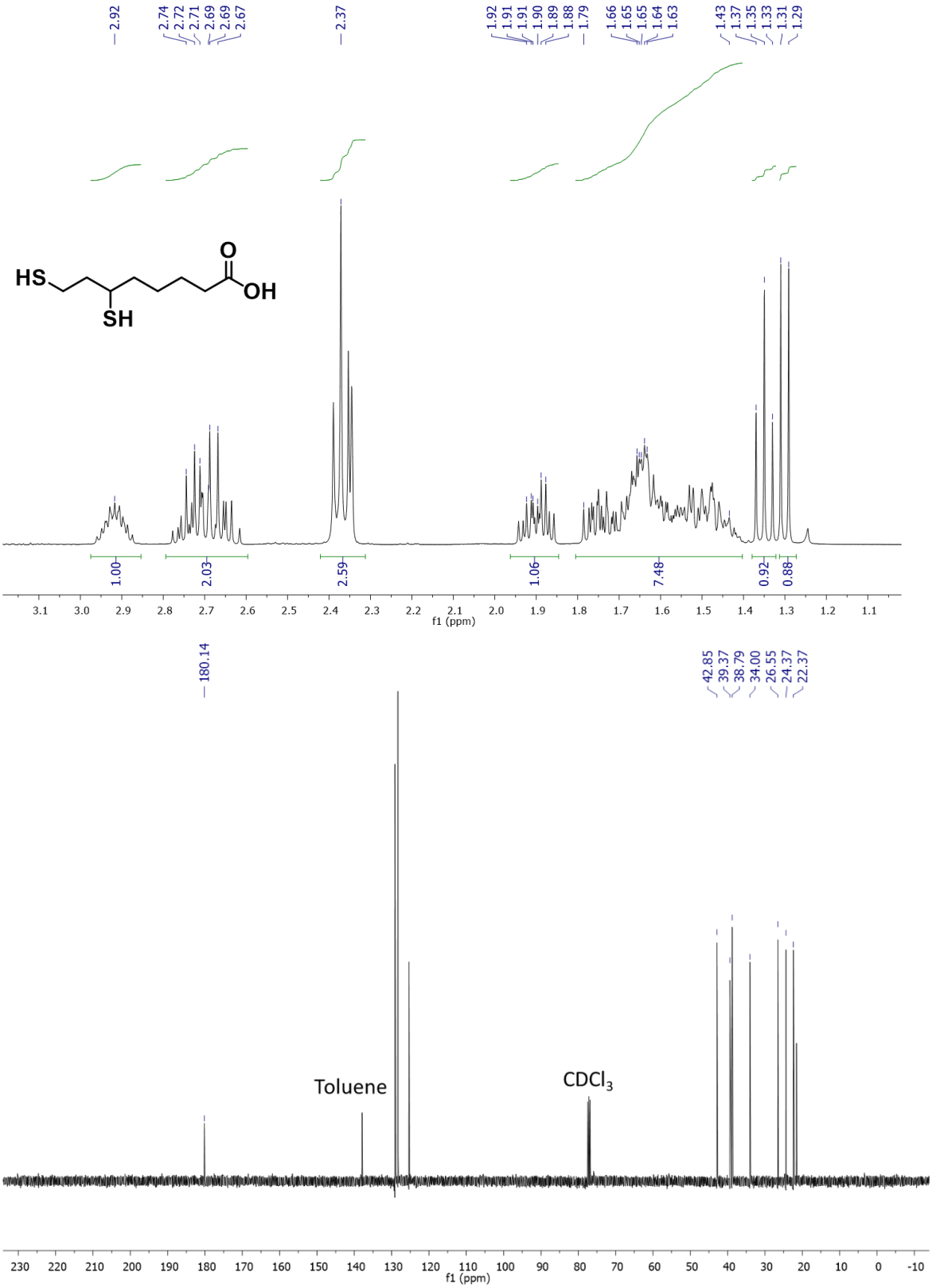

Comparison of ^{1}H-NMR spectra (DMSO-d6, 400 MHz) of CIS-DHLA, lipoic acid and DHLA

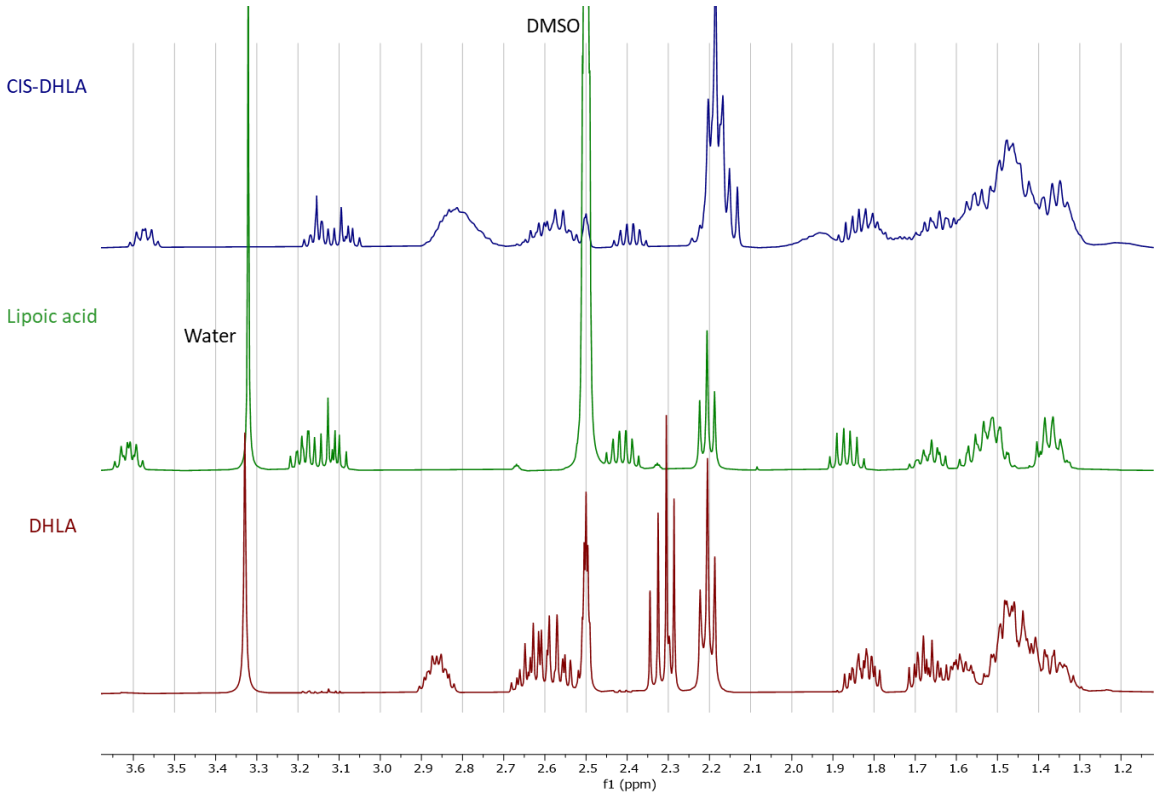

^{1}H-NMR spectrum (DMSO-d6, 400 MHz) of 1-octanethiol

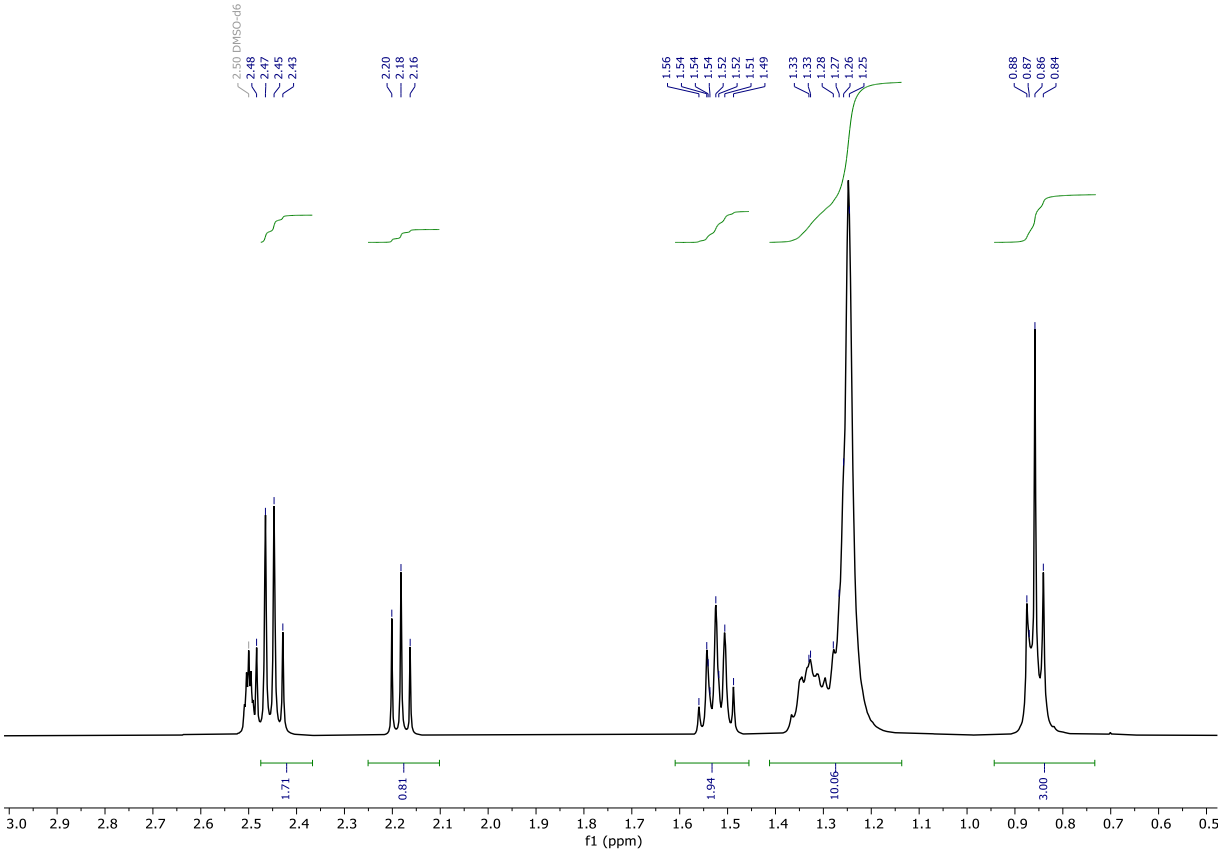

Scherrer equation

For the computation of the crystallites size inside the CIS QDs, the following formula was used:

$$d = \frac{K \cdot \lambda}{\beta \cdot cos\vartheta}$$

Where K, a shape factor, is set as 0.9; λ is the X-ray wavelength from Kα of Cu (0.154184 nm), β is the full width at half maximum of a certain peak (e.g., the peak at 2ϑ = 27°) expressed in rad and ϑ the Bragg angle (13.5°).

MP-AES measurements

Table S1: Results obtained via MP-AES on 1/50 of a sample of CIS_{4nm}-OT after purification and digestion in 9 mL of 7 M HNO_3. The resulting Cu/In ratio is 0.97, very close to the feeding solution. In addition to that, the amount of copper and indium detected after purification and digestion is 97% and 99% of the feeding amount, respectively. This confirms that the heating-up procedure is able to assure the almost total consumption of metal precursors, lowering their waste.

Cu (218 nm)	Cu (510 nm)	In (325 nm)	In (451 nm)
34.93 ppm	36.25 ppm	72.85 ppm	71.62 ppm
35.04 ppm	36.31 ppm	72.88 ppm	71.44 ppm
36.28 ppm	37.07 ppm	74.5 ppm	71.28 ppm

Determination of the energy gap of CIS samples

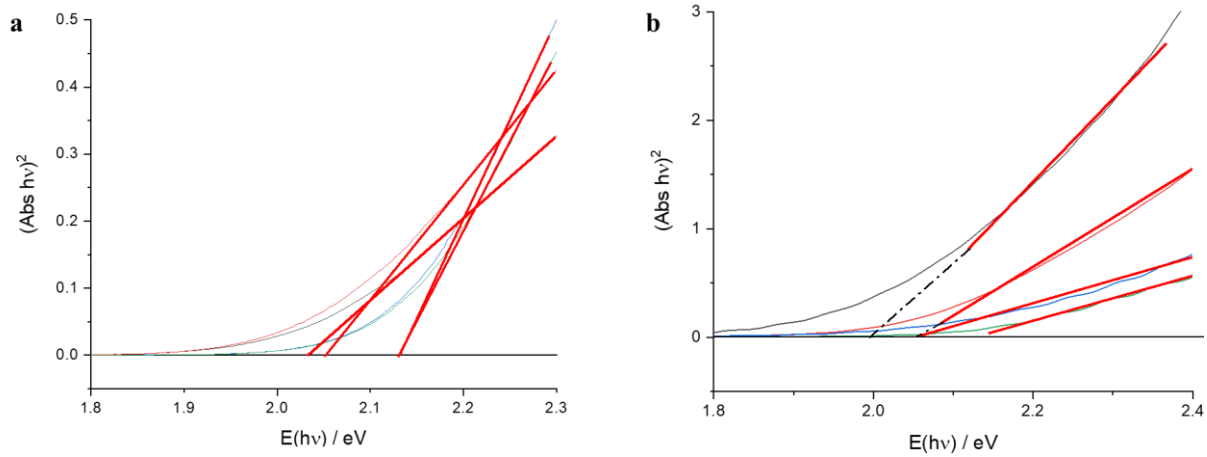

Figure S1 (a) Tauc Plot for CIS_{3nm}-OT (green line), CIS_{3nm}-DHLA (blue line); CIS_{4nm}-OT (red line) and CIS_{4nm}-DHLA (black line) in solution; (b) Tauc Plot for the direct transition of the photoanodes CIS_{3nm}/TiO_2 (green line), $CIS_{3nm}/CdS/TiO_2$ (blue line), CIS_{4nm}/TiO_2 (red line) and $CIS_{4nm}/CdS/TiO_2$ (black line).

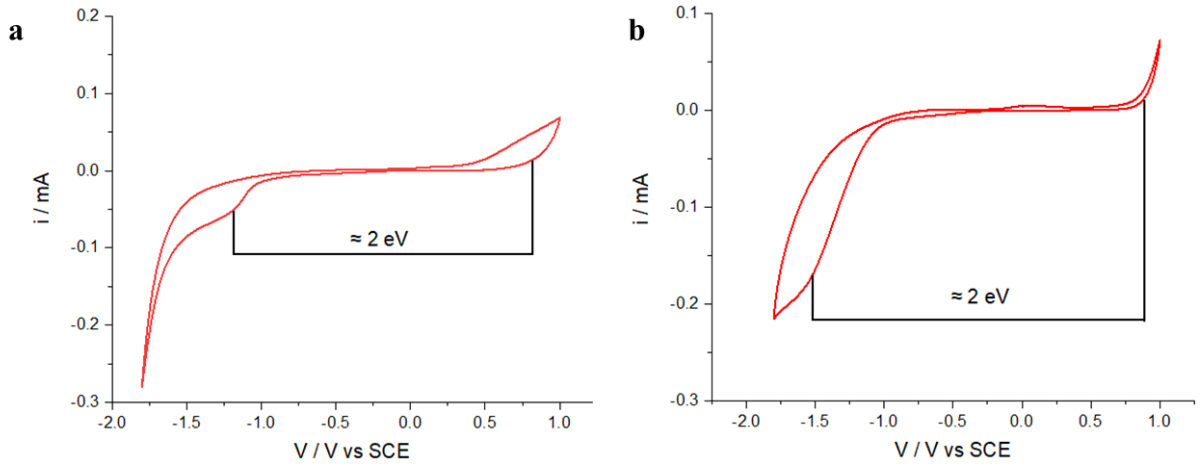

Figure S2 Cyclic voltammetries in dearated 0.1 M $LiClO_4$ in ACN -1.8 V to 1.0 V (vs SCE) on (a) CIS_{3nm} /ZrO_2 and (b) CIS_{4nm} /ZrO_2.

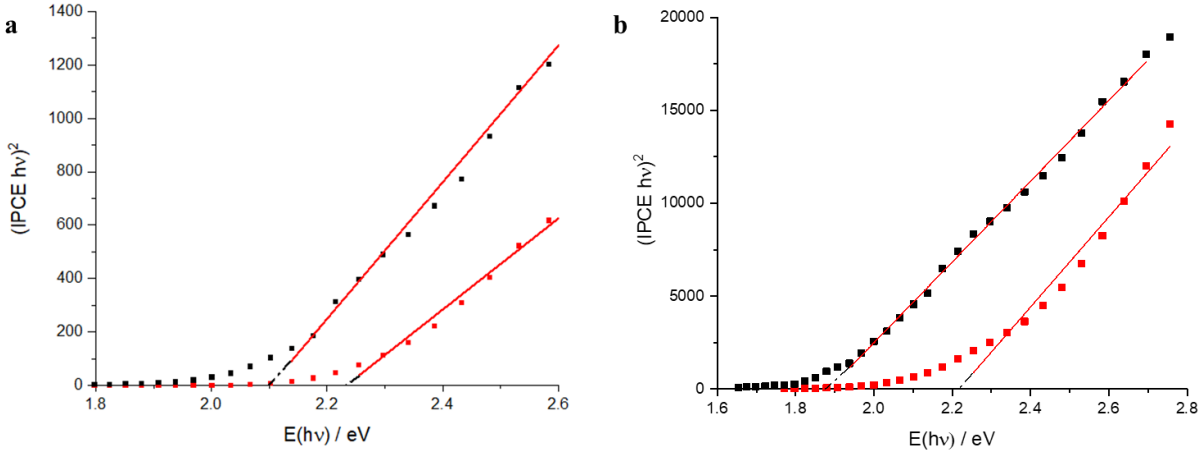

Figure S3 Tauc plots from IPCE data: (a) CIS_{3nm} /TiO_2 (red dots) and CIS_{4nm} /TiO_2 (black dots); (b) CIS_{3nm} /CdS/TiO_2 (red dots) and CIS_{4nm} /CdS/TiO_2 (black dots). Data collected from potentiostatic experiments at 0.2 V vs Ag in 0.5 M Na_2S.

SEM of photoanodes based on CIS QDs and CdS

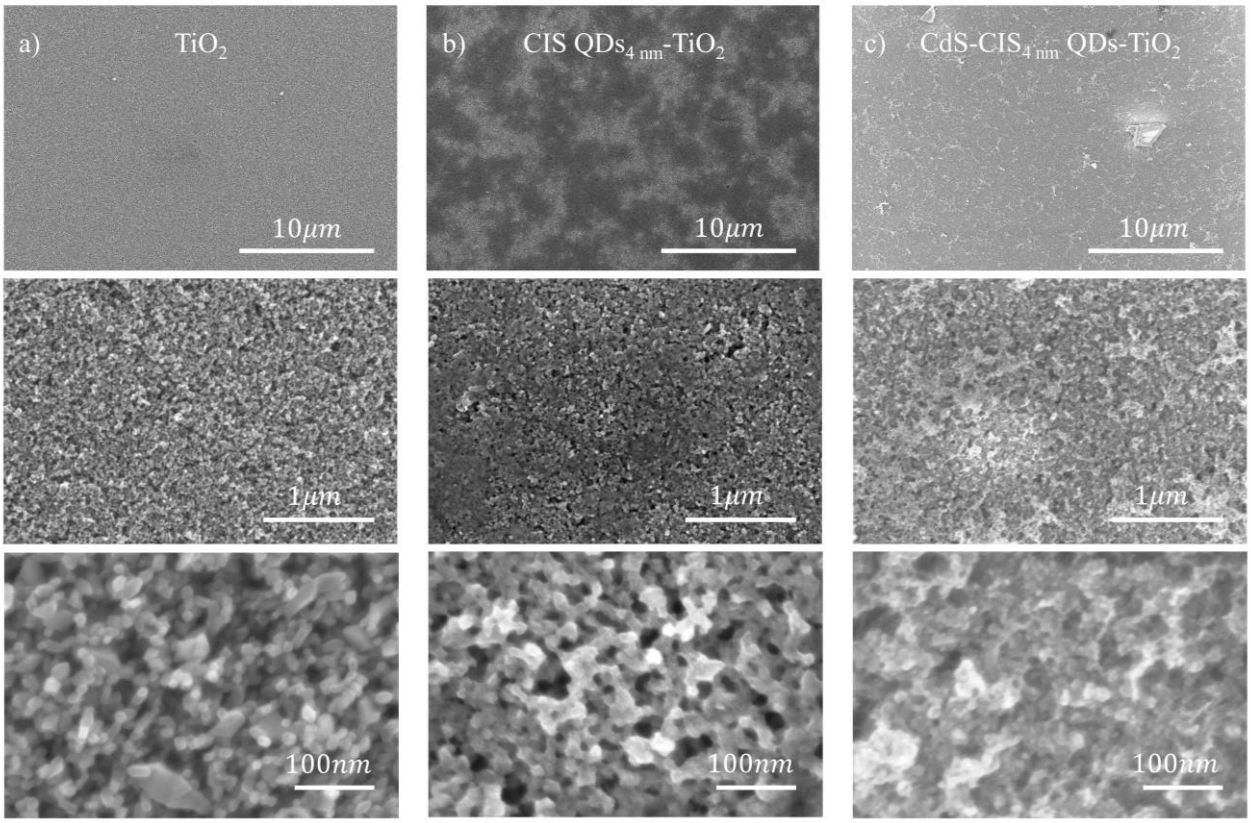

Figure S4 Increasing magnification SEM images of (a) bare TiO_2, (b) CIS_{4nm}/TiO_2 and (c) $CIS_{4nm}/CdS/TiO_2$ photoanodes.

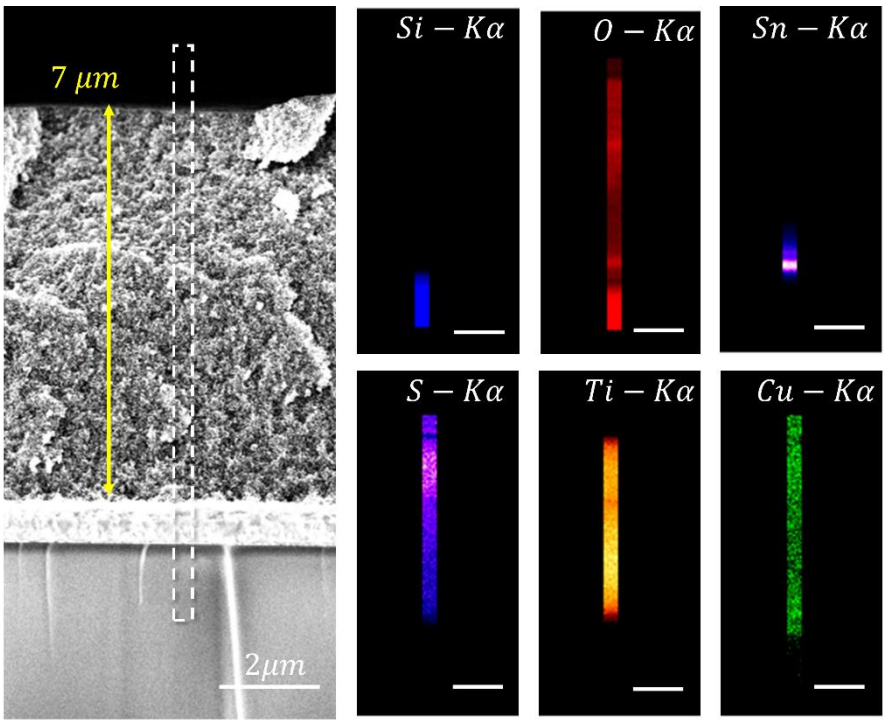

Figure S5 EDX mapping of a cross section of CIS_{4nm}/TiO_2 , exhibiting homogeneous distribution of Cu and S within the TiO_2 layer, with a slight increase of S content towards the surface. Si and Sn are reported to identify the FTO-glass substrate.

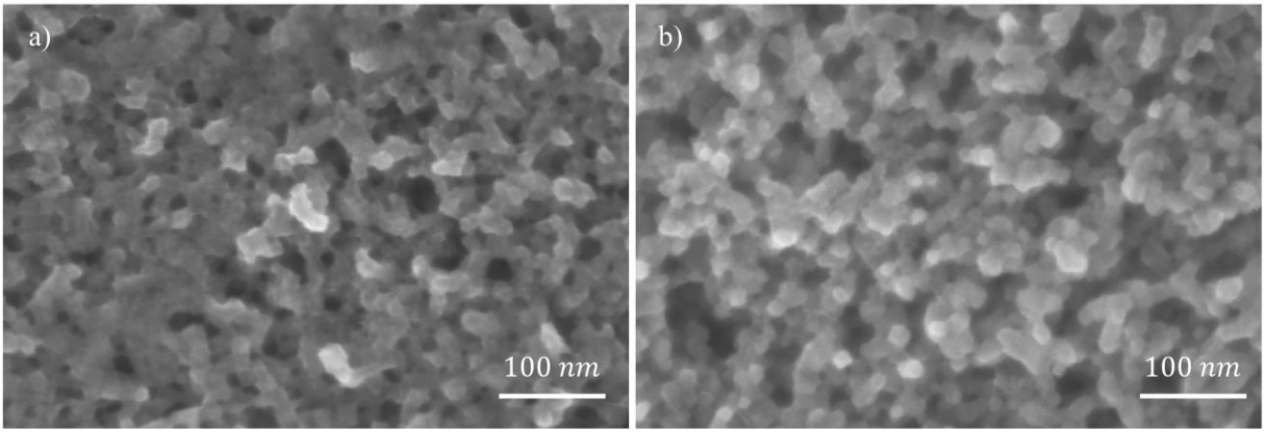

Figure S6 Comparison between SEM images of CIS_{4nm}/TiO_2 photoanode (a) before and (b) after 50 J-V cycles.

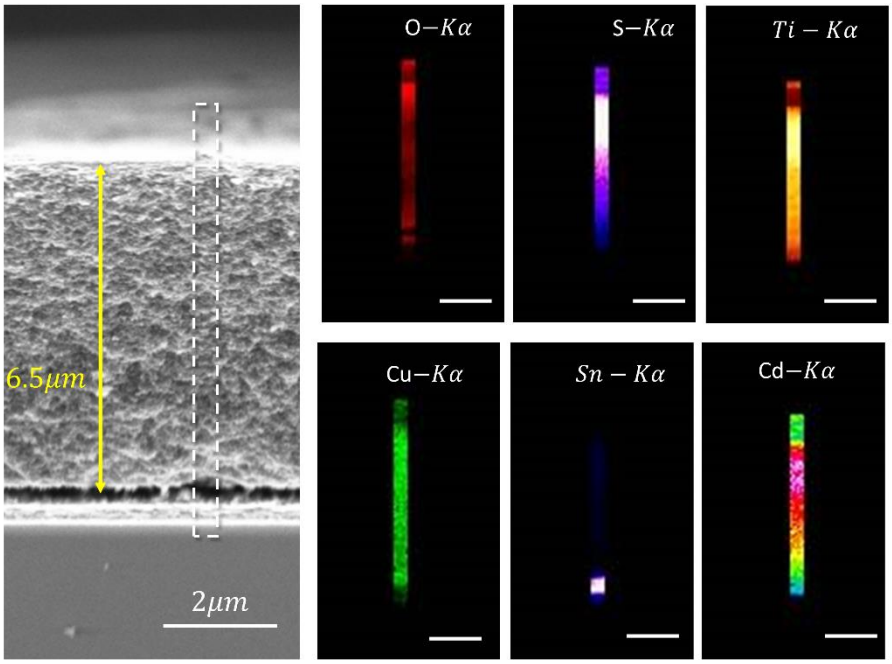

Figure S7 EDX mapping of a cross section of $CIS_{4nm}/CdS/TiO_2$ photoanode, exhibiting homogeneous distribution of Cd and S within the TiO_2 layer, with a slight increase of Cd and S content towards the surface. Sn is reported to identify the FTO back contact.

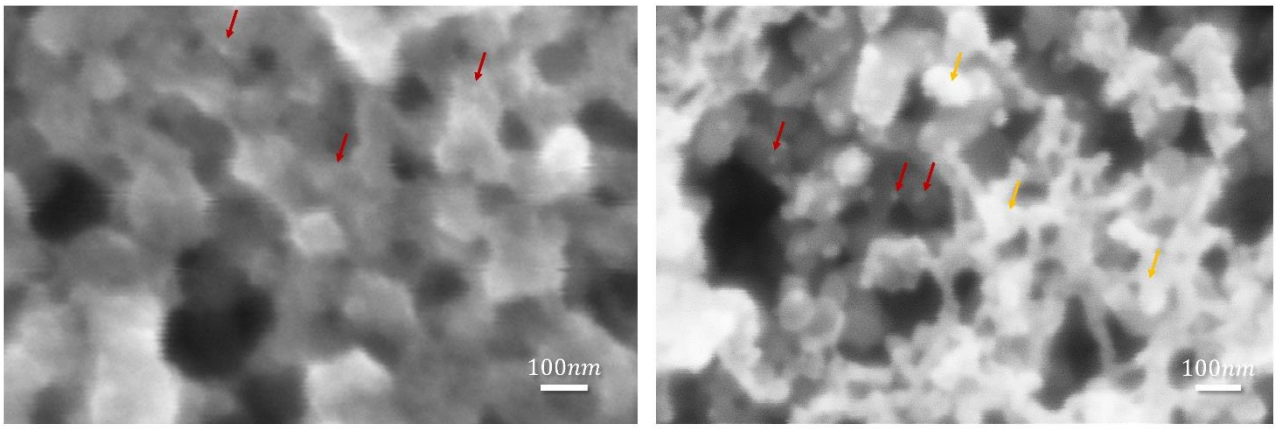

Figure S8 High magnification SEM micrographs of a) CIS_{4nm}/TiO_2 and $CIS_{4nm}/CdS/TiO_2$ samples, with arrows highlighting CIS nanoparticles (red) and CdS overlayer structures (orange).

Table S2 Atomic composition of the different photoanodes. The EDX analyses were performed on a large area of the samples to avoid distribution issues. The comparison highlights a constant presence of titania and confirms the presence of the CIS_{4nm} QDs (Cu, In and S), as well as the CdS layer, when deposited. No variation of composition is appreciated in the sample CIS_{4nm}/TiO_2 after J/V cycles.

Electrode / **Element**	TiO_2	CIS/TiO_2 before 50 J/V cycles	CIS/TiO_2 after 50 J/V cycles	$CIS/CdS/TiO_2$	CdS/TiO_2
C (K line)	1.72	8.06	4.68	6.14	-
O (K line)	72.50	64.22	66.35	58.48	73.29
Si (K line)	0.05	0.04	0.18	0.09	0.12
Ti (K line)	25.58	22.38	24.58	20.86	24.36
Sn (K line)	1.72	0.18	0.23	-	0.15
Cu (L line)	-	1.43	0.93	0.83	-
In (L line)	-	1.08	0.96	1.05	-
S (L line)	-	2.68	2.13	5.43	0.97
Cd (L line)	-	-	-	3.86	1.10

Electrochemical treatment of CIS/TiO_2 photoanodes

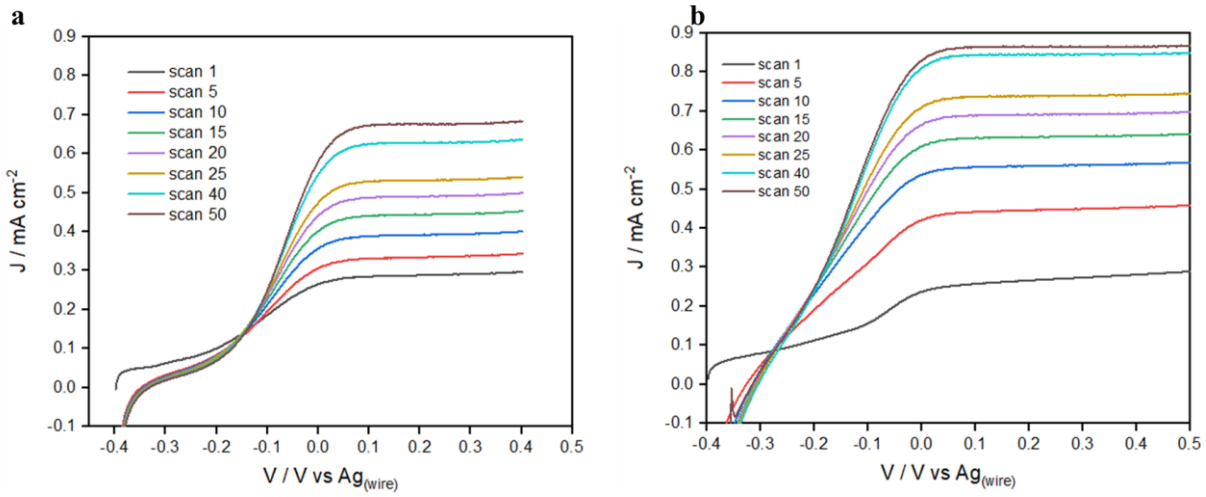

Figure S9 J/V curves of CIS_{3nm}/TiO_2 (a) and CIS_{4nm}/TiO_2 (b) photoanodes in the presence of a 455-nm cutoff after various J/V cycles.

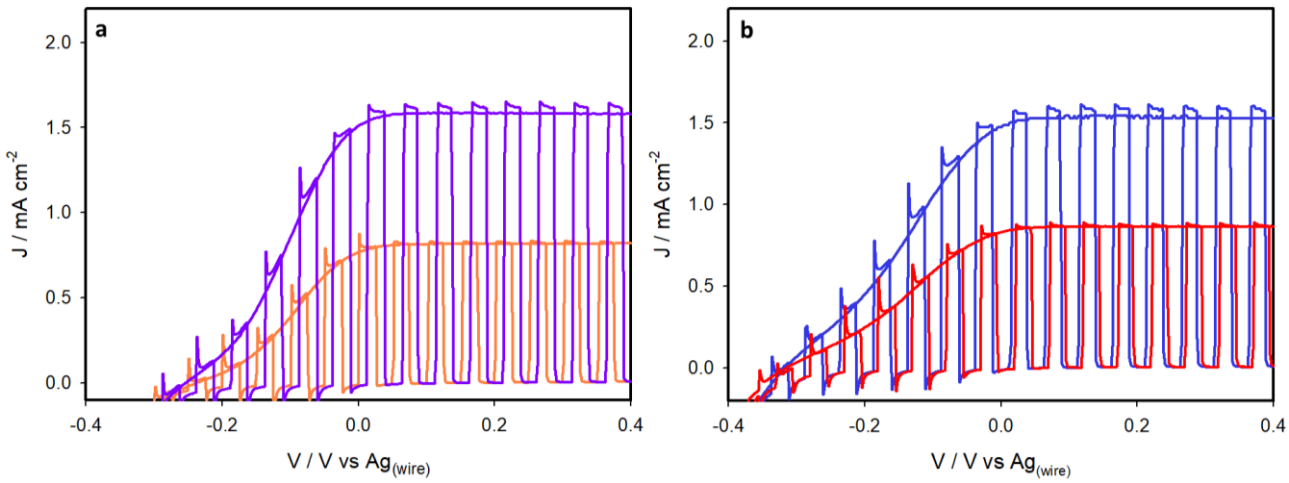

Figure S10 Linear and chopped J/V curves of (a) CIS_{3nm}/TiO_2 and (b) CIS_{4nm}/TiO_2 photoanodes after 50 cycles in 1.0 M aqueous Na_2S in the presence (orange and red lines) or absence (violet and blue lines) of a 455-nm cutoff filter, under 1-sun equivalent irradiation.

Effect of SILAR cycles on current density

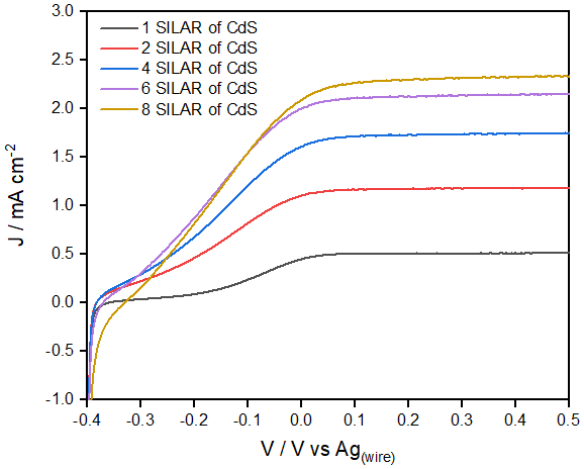

Figure S11 J/V curves of CdS-CIS_{3nm} QDs-TiO_2 photoanodes in the presence of a 455-nm cutoff after 1, 2, 4, 6 and 8 SILAR cycles in aqueous $Cd(NO_3)_2$ and Na_2S 0.1 M.

Absorption spectrum of CIS/CdS electrodes

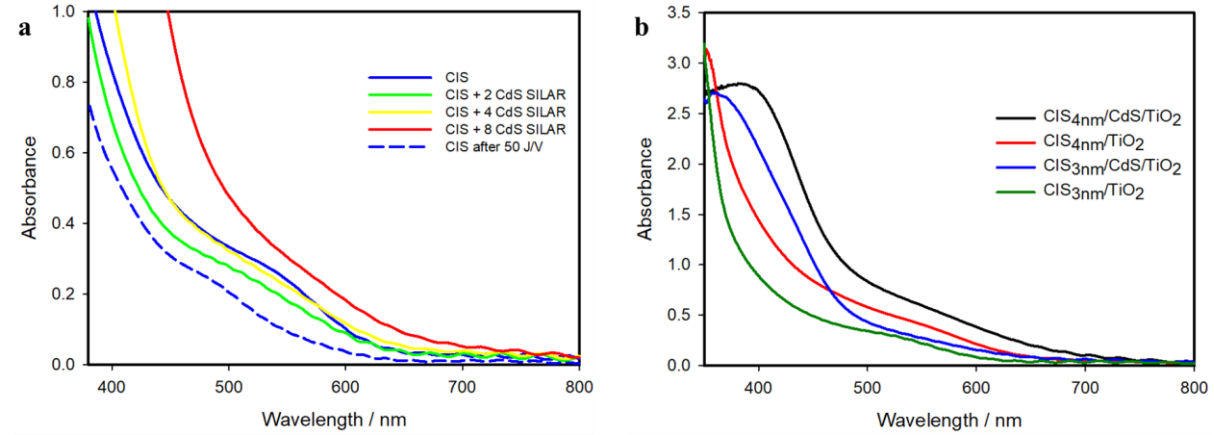

Figure S12 (a) Absorption spectra of CIS_{3nm}/TiO_2 after the deposition of the CIS QDs overnight (straight blue line) or after 50 J/V cycles (dashed blue line) and after 2 (green line), 4 (yellow

line) and 8 (red line) SILAR cycles in 0.1 M $Cd(NO_3)_{2\,(aq)}$ and 0.1 M $Na_2S_{(aq)}$, (b) Absorption spectra of CIS_{3nm}/TiO_2 (green line), $CIS_{3nm}/CdS/TiO_2$ (blue line), CIS_{4nm}/TiO_2 (red line) and $CIS_{4nm}/CdS/TiO_2$ (black line).

Comparison with bare CdS/TiO_2 electrodes

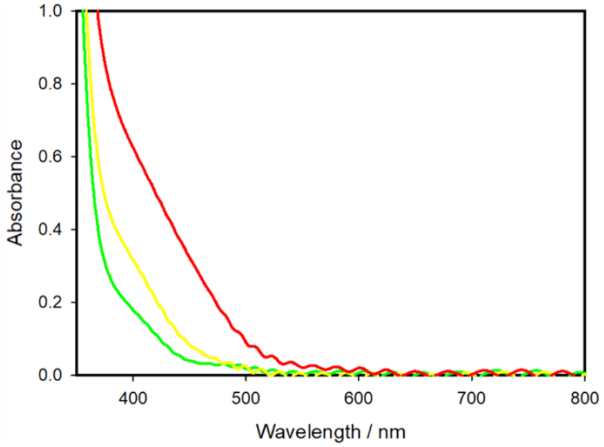

Figure S13 Absorption spectra of the photoanodes based on bare CdS after 2 (green line), 4 (yellow line) and 8 (red line) SILAR cycles in 0.1 M $Cd(NO_3)_{2\,(aq)}$ and 0.1 M $Na_2S_{\,(aq)}$.

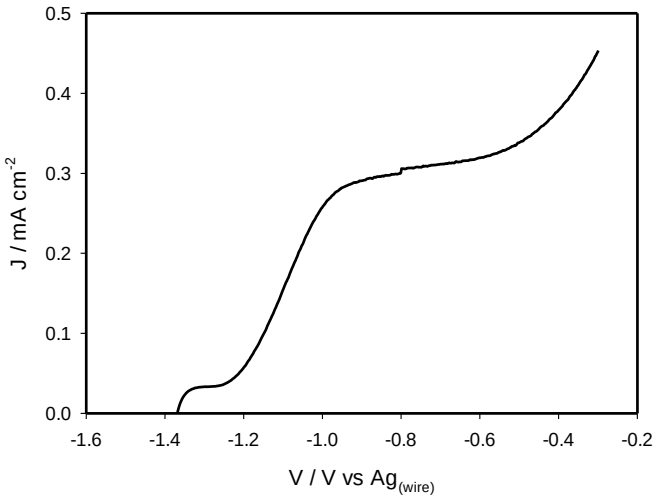

Figure S14 J/V curve of the photoanode based on CdS deposited after 8 SILAR cycles in $Cd(NO_3)_2$ and Na_2S in the presence of a 455-nm cutoff filter.

Stability of the electrodes

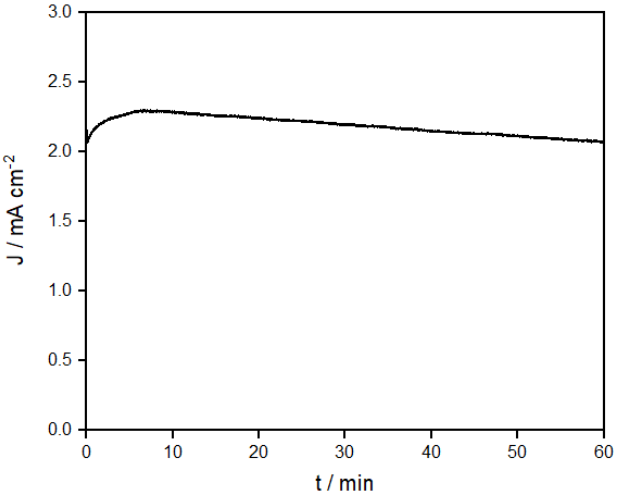

Figure S15 Chronoamperometrie of CIS_{3nm}/CdS photoanodes at 0.1 V vs Ag QRE.

Time-resolved measurements

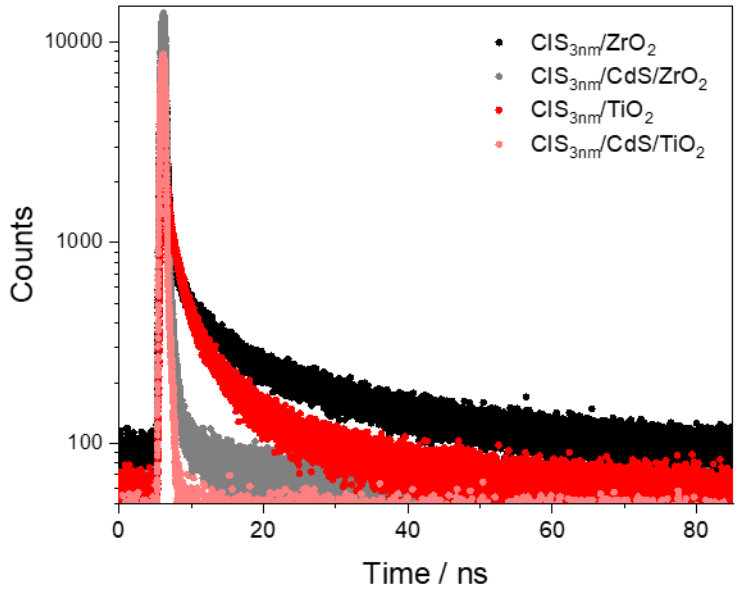

Figure S9 Separated charge state lifetime for CIS_{3nm}/ZrO_2 (black dots, $<\tau>$ = 8.7 ns), $CIS_{3nm}/CdS/ZrO_2$ (grey dots, $<\tau>$ < 300 ps), CIS_{3nm}/TiO_2 (red dots, $<\tau>$ = 3.4 ns) and $CIS_{3nm}/CdS/TiO_2$ electrodes ($<\tau>$ < 300 ps pink dots).

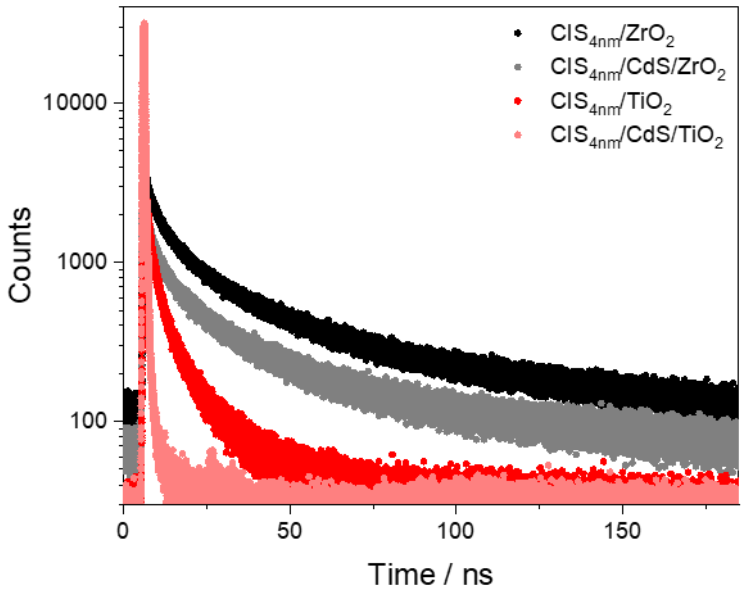

Figure S10 Separated charge state lifetime for CIS_{4nm}/ZrO_2 (black dots, $<\tau>$ = 15.3 ns), $IS_{4nm}/CdS/ZrO_2$ (grey dots, $<\tau>$ = 13.8 ns), CIS_{4nm}/TiO_2 (red dots, $<\tau>$ = 3.8 ns) and $CIS_{4nm}/CdS/TiO_2$ electrodes (pink dots, $<\tau>$ = 0.58 ns).

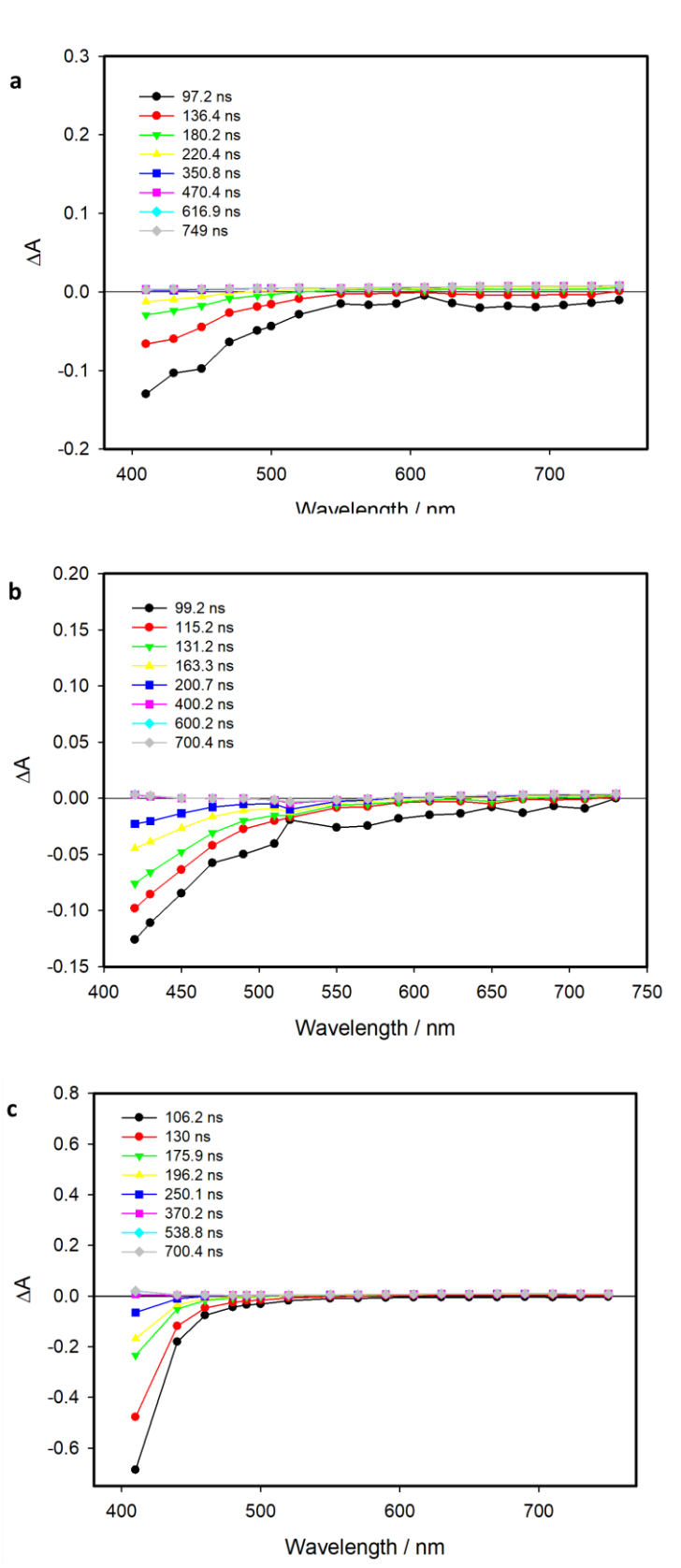

Figure S18 Transient absorption spectroscopy data of (a) CIS_{3nm}/TiO_2 recorded in NaOH solution 0.01 M, (b) CIS_{3nm}/TiO_2 recorded in Na_2S 1 M and (c) $CIS_{3nm}/CdS/TiO_2$ recorded in Na_2S 1 M. Inset: enlarged view.